

Unitarity and Bounds on the Scale of Fermion Mass Generation

R. Sekhar Chivukula,* Neil D. Christensen,† Baradhwaj Coleppa,‡ and Elizabeth H. Simmons§

*Department of Physics and Astronomy
Michigan State University
East Lansing, MI 48824*

(Dated: July 30, 2018)

The scale of fermion mass generation can, as shown by Appelquist and Chanowitz, be bounded *from above* by relating it to the scale of unitarity violation in the helicity nonconserving amplitude for fermion-anti-fermion pairs to scatter into pairs of longitudinally polarized electroweak gauge bosons. In this paper, we examine the process $t\bar{t} \rightarrow W_L^+ W_L^-$ in a family of phenomenologically-viable deconstructed Higgsless models and we show that scale of unitarity violation depends on the mass of the additional vector-like fermion states that occur in these theories (the states that are the deconstructed analogs of Kaluza-Klein partners of the ordinary fermions in a five-dimensional theory). For sufficiently light vector fermions, and for a deconstructed theory with sufficiently many lattice sites (that is, sufficiently close to the continuum limit), the Appelquist-Chanowitz bound can be substantially weakened. More precisely, we find that, as one varies the mass of the vector-like fermion for fixed top-quark and gauge-boson masses, the bound on the scale of top-quark mass generation interpolates smoothly between the Appelquist-Chanowitz bound and one that can, potentially, be much higher. In these theories, therefore, the bound on the scale of fermion mass generation is independent of the bound on the scale of gauge-boson mass generation. While our analysis focuses on deconstructed Higgsless models, any theory in which top-quark mass generation proceeds via the mixing of chiral and vector fermions will give similar results.

I. INTRODUCTION

Although the mechanism of electroweak symmetry breaking remains a mystery, it is clear that this mechanism must give mass to two very different classes of particles: the electroweak gauge bosons and the fermions. In the standard model, the scalar Higgs [1] doublet couples directly to both classes of particles [2, 3]. Moreover, the gauge and Yukawa couplings through which the Higgs interacts, respectively, with gauge bosons and fermions are proportional to the masses generated for those states when the scalar doublet acquires a vacuum expectation value. Nonetheless, in considering physics beyond the standard model, the possibility remains that the gauge boson and fermion masses are generated through different mechanisms. In particular, it is possible that electroweak symmetry breaking is transmitted to the fermions via some intermediary physics specifically associated with fermion mass generation.

Appelquist and Chanowitz [4] have shown¹ that the tree-level, spin-0 scattering amplitude for fermion-anti-fermion pairs to scatter into longitudinally-polarized electroweak gauge bosons grows linearly with energy below the scale of the physics responsible for transmitting electroweak symmetry breaking to the fermions. As the amplitude must be unitary, one can derive an *upper* bound on the scale of fermion mass generation by finding the

energy at which the amplitude would grow to be of order $1/2$. The rate of energy growth is proportional to the mass of the fermions involved. The most stringent bound, therefore, arises from top-quark annihilation, and the bound on the scale of top-quark mass generation is found to be of order a few TeV.²

As emphasized by Golden [6], the interpretation of the Appelquist-Chanowitz (AC) bound on the scale of top-quark mass generation can be problematic: longitudinal electroweak gauge-boson elastic scattering itself grows quadratically with energy [9, 10, 11, 12, 13] below the scale of the physics responsible for electroweak gauge-boson mass generation. As the scale of the physics responsible for electroweak symmetry breaking is also bounded by of order a TeV, it can be difficult to be sure that the violation of unitarity in fermion annihilation is truly independent of the violation of unitarity in the gauge-boson sector. The standard model illustrates this difficulty, as in that case the Higgs boson is responsible for restoring unitarity in *both* the fermion annihilation and gauge-boson scattering processes.

In this paper, we discuss unitarity violation and the resulting bounds on the scale of top-quark mass generation in the context of deconstructed Higgsless models. Higgsless models [14] achieve electroweak symmetry breaking without introducing a fundamental scalar Higgs boson [1], and the unitarity of longitudinally-polarized W and Z boson scattering [9, 10, 11, 12, 13] is preserved

*email: sekhar@msu.edu

†email: neil@pa.msu.edu

‡email: baradhwaj@pa.msu.edu

§email: esimmons@msu.edu

¹ See also [5, 6].

² For light fermions, the scattering of fermions into many gauge-bosons yields a stronger result than the Appelquist-Chanowitz bound [7, 8]. For the top-quark, however, two-body final states yield the strongest bound.

by the exchange of extra vector bosons [15, 16, 17, 18]. Inspired by TeV-scale [19] compactified five-dimensional gauge theories [20, 21, 22, 23], these models provide effectively unitary descriptions of the electroweak sector beyond 1 TeV. Deconstruction [24, 25] is a technique to build a four-dimensional gauge theory, with an appropriate gauge-symmetry breaking pattern, which approximates the properties of a five-dimensional theory. Deconstructed Higgsless models [26, 27, 28, 29, 30, 31, 32] have been used as tools to compute the general properties of Higgsless theories, and to illustrate the phenomenological properties of this class of models.

The simplest deconstructed Higgsless model [33, 34] incorporates only three sites on the deconstructed lattice, and the only additional vector states (other than the usual electroweak gauge bosons) are a triplet of vector bosons. While simple, the three site model is sufficiently rich to describe the physics associated with fermion mass generation, as well as the fermion delocalization [35, 36, 37, 38, 39, 40, 41, 42] required in order to accord with precision electroweak tests [43, 44, 45, 46, 47]. It is straightforward to generalize this model to an arbitrary number of sites [49]. In the continuum limit (the limit in which the number of sites goes to infinity), this model reproduces the five-dimensional model introduced in [39].

A fermion field in a general compactified five-dimensional theory gives rise to a tower of Kaluza-Klein (KK) modes, the lightest of which can (under chiral boundary conditions) be massless in the absence of electroweak symmetry breaking. The lightest states can therefore be identified with the ordinary fermions. The massive Kaluza-Klein fermion modes are, however, massive Dirac fermions from the four-dimensional point of view. Correspondingly, the fermions in a deconstructed Higgsless model include both chiral and vector-like electroweak states [33, 49], and generation of the masses of the ordinary fermions in these models involves the mixing of the chiral and vector states [37, 38]. As we will demonstrate, the scale of top-quark mass generation in these models depends on the masses of the vector-like fermions (the “KK” modes), as well as on the number of sites in the deconstructed lattice.

What is particularly interesting about deconstructed Higgsless models, in this context, is that one *can* distinguish between the unitarity-derived bounds on the scales of gauge-boson and top-quark mass generation. We will demonstrate that, for an appropriate number of deconstructed lattice sites, spin-0 top-quark annihilation to longitudinally-polarized gauge-bosons remains unitary at tree-level up to energies much higher than the naive AC bound if the vector-like fermions are light. However the AC bound is reproduced as the mass of the vector-like fermion is increased. Therefore, for fixed top-quark and gauge-boson masses, the bound on the scale of fermion mass generation interpolates smoothly between the AC bound and one that can, potentially, be much higher as the mass of the vector-like fermion varies. The unitarity bounds on elastic scattering of longitudinal electroweak

gauge bosons in Higgsless models [48], however, depend only on the masses of the gauge-boson KK modes. In this sense, the bound on the scale of fermion mass generation is *independent* of the bound on the scale of gauge-boson mass generation.

While our discussion is restricted to deconstructed Higgsless models, many models of dynamical electroweak symmetry breaking incorporate the mixing of chiral and vector fermions to accommodate top-quark mass generation. Examples include the top-quark seesaw model [50, 51, 52], and models in which the top mixes with composite fermions arising from a dynamical electroweak symmetry breaking sector [53, 54, 55]. Indeed, the fermion delocalization required to construct a realistic Higgsless model is naturally interpreted, in the context of AdS/CFT duality [56, 57, 58, 59], as mixing between fundamental and composite fermions [60]. As chiral-vector fermion mixing is the basic feature required for our results, we expect similar effects in these other models.

In the next section, to set notation and make contact with the literature, we reproduce [6] the Appelquist-Chanowitz bound in the electroweak chiral Lagrangian [61, 62, 63, 64, 65] — which may be interpreted as a “two-site” Higgsless model. In section three, we introduce the $n(+2)$ site Higgsless models that we will use for our calculations. Section four contains our calculations and primary results. The last section summarizes our findings.

II. THE APPELQUIST-CHANOWITZ BOUND

In the standard model (SM), the helicity non-conserving process $t_+\bar{t}_+ \rightarrow W_L^+W_L^-$ receives contributions at tree level from the diagrams in Figure 1. We are interested in the behavior of the amplitude for large center of mass energy, $\sqrt{s} \gg M_W, m_t$. This allows us to expand the amplitude in the small parameters M_W^2/s and m_t^2/s . Practically, this means that we use the following leading order approximations. For the longitudinal polarization of the W gauge boson, we use

$$\epsilon_{W_L}^\mu \simeq \frac{k_{W_L}^\mu}{M_W}, \quad (1)$$

where $k_{W_L}^\mu$ is the four-momentum of the corresponding boson. For the spinor chain in the s channel, we use

$$\bar{v}_+(\not{k}_1 - \not{k}_2)(g_L P_L + g_R P_R)u_+ \simeq m_t \sqrt{s} \cos \theta (g_L + g_R) \quad (2)$$

$$\bar{v}_-(\not{k}_1 - \not{k}_2)(g_L P_L + g_R P_R)u_- \simeq -m_t \sqrt{s} \cos \theta (g_L + g_R), \quad (3)$$

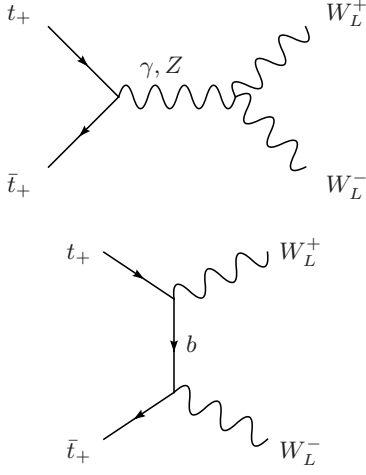


FIG. 1: The diagrams that contribute to the process $t_+ \bar{t}_+ \rightarrow W_L^+ W_L^-$ in the Higgsless SM. There are analogous diagrams for the process $t_- \bar{t}_- \rightarrow W_L^+ W_L^-$. Each diagram has an amplitude that grows linearly with \sqrt{s} for all energies. However, most (but not all) of this linear \sqrt{s} growth cancels when the diagrams are summed. The remaining piece that grows linearly with \sqrt{s} comes from the t channel diagram, and it eventually surpasses the unitarity bound. In the SM, this unitarity violation is eliminated by the contribution of the Higgs in the s channel.

where k_1^μ and k_2^ν are the momenta of the outgoing bosons, and for the spinor chain in the t channel we find

$$\bar{v}_+ \not{k}_2 (\not{p}_1 - \not{k}_1) \not{k}_1 g_L P_L u_+ \simeq \frac{m_t t \sqrt{s}}{2} (1 + \cos \theta) g_L \quad (4)$$

$$\bar{v}_- \not{k}_2 (\not{p}_1 - \not{k}_1) \not{k}_1 g_L P_L u_- \simeq -\frac{m_t t \sqrt{s}}{2} (1 + \cos \theta) g_L \quad (5)$$

where

$$P_L = \frac{1}{2} (1 - \gamma_5) \quad (6)$$

$$P_R = \frac{1}{2} (1 + \gamma_5) \quad (7)$$

are chirality projection operators, and g_L and g_R are chiral electroweak coupling constants.

Since the $t\bar{t} \rightarrow W^+ W^-$ amplitude is the same for each color and only differs by a sign for the opposite helicity, we get the largest amplitude by considering the incoming state³

$$|\psi\rangle = \frac{1}{\sqrt{6}} \left(|\bar{t}_{1+} t_{1+}\rangle + |\bar{t}_{2+} t_{2+}\rangle + |\bar{t}_{3+} t_{3+}\rangle - |\bar{t}_{1-} t_{1-}\rangle - |\bar{t}_{2-} t_{2-}\rangle - |\bar{t}_{3-} t_{3-}\rangle \right), \quad (8)$$

³ The state we consider here differs from that chosen by [4], as we include both combinations of incoming helicities. This state allows us to derive a slightly stronger bound, *c.f.* Eqn (23).

where the numerical subscripts (1,2, and 3) label the three different colors. Putting the pieces together gives the scattering amplitude

$$\begin{aligned} \mathcal{M}(\psi \rightarrow W_L W_L) &= \frac{\sqrt{6} m_t \sqrt{s} \cos \theta}{2M_W^2} \quad (9) \\ &\times \left(2g_{tt\gamma} g_{\gamma WW} + g_{LttZ} g_{ZWW} + g_{RttZ} g_{ZWW} - g_{LtbW}^2 \right) \\ &+ \frac{\sqrt{6} m_t \sqrt{s}}{2M_W^2} g_{LtbW}^2, \end{aligned}$$

for $\sqrt{s} \gg M_W, m_t$, where the electroweak couplings are given by⁴

$$g_{tt\gamma} = \frac{2}{3} e, \quad (10)$$

$$g_{\gamma WW} = e, \quad (11)$$

$$g_{LttZ} = \frac{e}{\sin \theta_W \cos \theta_W} \left(\frac{1}{2} - \frac{2}{3} \sin^2 \theta_W \right), \quad (12)$$

$$g_{RttZ} = \frac{e}{\sin \theta_W \cos \theta_W} \left(-\frac{2}{3} \sin^2 \theta_W \right), \quad (13)$$

$$g_{ZWW} = \frac{e \cos \theta_W}{\sin \theta_W}, \quad (14)$$

$$g_{LtbW} = \frac{e}{\sqrt{2} \sin \theta_W}. \quad (15)$$

With these couplings, we find the identity

$$2g_{tt\gamma} g_{\gamma WW} + g_{LttZ} g_{ZWW} + g_{RttZ} g_{ZWW} - g_{LtbW}^2 = 0. \quad (16)$$

The remaining amplitude is, therefore,

$$\mathcal{M} = \frac{\sqrt{6} m_t \sqrt{s}}{2M_W^2} g_{LtbW}^2 \quad (17)$$

which grows linearly with \sqrt{s} for $\sqrt{s} \gg M_W, m_t$. We note that $g_{LtbW} = g/\sqrt{2}$ and $M_W = gv/2$, where g is the weak coupling and $v \simeq 246$ GeV is the weak scale, giving [4]

$$\mathcal{M} = \frac{\sqrt{6} m_t \sqrt{s}}{v^2}. \quad (18)$$

We can check using the equivalence theorem [11, 68], where one replaces the longitudinal gauge-bosons by the corresponding ‘‘eaten’’ Nambu-Goldstone Bosons. In this limit, the only diagram that contributes to the $J = 0$ amplitude is shown in Figure 2. The leading order approximations

$$\bar{v}_+ u_+ \simeq \sqrt{s} \quad \bar{v}_- u_- \simeq -\sqrt{s} \quad (19)$$

⁴ Our expression here differs in the sign of the term proportional to g_{LtbW}^2 from that given in [4], and is correct for the top-quark which is the $T_3 = +1/2$ member of an electroweak doublet. The corresponding expression in [4], which is from [66, 67], is correct for the *lower* member of an electroweak doublet with $T_3 = -1/2$.

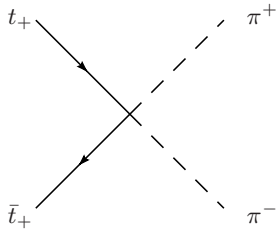


FIG. 2: The diagram that contributes linear growth in \sqrt{s} to the process $t_+ \bar{t}_+ \rightarrow \pi^+ \pi^-$ in the Higgsless SM, where we have used the equivalence theorem to replace the longitudinally polarized gauge-boson by the corresponding “eaten” Goldstone Bosons. There is an analogous diagram for the process $t_- \bar{t}_- \rightarrow \pi^+ \pi^-$.

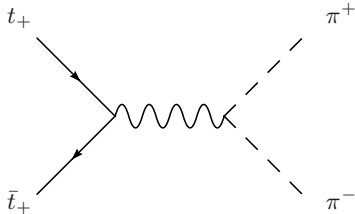


FIG. 3: This diagram, corresponding to s -channel Z -boson exchange in the equivalence-theorem limit, *does not* contribute to the $J = 0$ partial wave scattering amplitude for the process $t_+ \bar{t}_+ \rightarrow \pi^+ \pi^-$ in the Higgsless SM.

combined with the four point coupling

$$g_{tt\pi^+\pi^-} = \frac{m_t}{v^2} \quad (20)$$

yield the same amplitude as in Eqn. (18)

$$\mathcal{M} = \frac{\sqrt{6} m_t \sqrt{s}}{v^2}. \quad (21)$$

Note that the potential s -channel contribution, illustrated in Figure 3, does *not* contribute in the $J = 0$ channel.

The $J = 0$ partial wave is extracted from Eqn. (18) as

$$a_0 = \frac{1}{32\pi} \int_{-1}^1 d\cos\theta \mathcal{M} = \frac{m_t \sqrt{6s}}{16\pi v^2} \quad (22)$$

To satisfy partial wave unitarity, this tree-level amplitude must be less than $1/2$, the maximum value for the real part of any amplitude lying in the Argand circle. This produces the bound

$$\sqrt{s} \lesssim \frac{8\pi v^2}{m_t \sqrt{6}} \approx 3.5 \text{ TeV}. \quad (23)$$

Our result differs numerically from that given in [4], as we include both helicity channels in Eq. 8, and bound the amplitude by $1/2$ rather than 1 .⁵

⁵ One may obtain a slightly stronger upper bound by considering

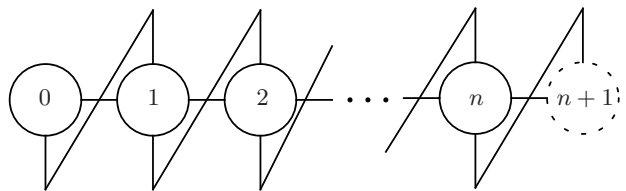


FIG. 4: Moose [69] diagram of the $n(+2)$ site model. Each solid (dashed) circle represents an $SU(2)$ ($U(1)$) gauge group. Each horizontal line is a non-linear sigma model. Vertical lines are fermions, and diagonal lines represent Yukawa couplings.

III. THE $n(+2)$ SITE DECONSTRUCTED HIGGSLESS MODEL

We will be studying the Higgsless model introduced in [49], denoted the $n(+2)$ site model. As we will discuss in subsection III A, the gauge sector is an $SU(2)^{n+1} \times U(1)$ extended electroweak group; the label n thus denotes how many extra $SU(2)$ groups the model contains relative to the Standard Model. The electroweak chiral lagrangian [61, 62, 63, 64, 65] can be obtained by setting $n = 0$ while the Higgsless Three Site Model [33], which has one extra $SU(2)$ group, can be obtained by setting $n = 1$. This model may be schematically represented by a “Moose” diagram [69] as shown in Figure 4. After discussing the gauge sector, we examine the fermion sector (subsection III B), the “eaten Nambu-Goldstone bosons” (subsection III C) and then the couplings that are relevant to our calculation of $t\bar{t} \rightarrow W^+ W^-$.

A. Gauge Boson Sector

The gauge group of the $n(+2)$ site model, as illustrated in Figure 4, is

$$G = SU(2)_0 \times \prod_{j=1}^n SU(2)_j \times U(1)_{n+1} \quad (24)$$

where $SU(2)_0$ is represented by the leftmost circle and has coupling g ; the gauge groups $SU(2)_j$ are represented consecutively by the internal circles and have a common coupling⁶ \tilde{g} ; and $U(1)_{n+1}$ is represented by the dashed circle at the far right and has coupling g' . The coupling

an isosinglet, spin-0, final state ($I = J = 0$) of gauge-bosons [5]. This amounts to a reduction in the value of the upper bound in Eqn. (23) by a factor of $\sqrt{2/3} \approx 0.8$.

⁶ Common couplings for the “internal” $SU(2)$ groups corresponds to a continuum model with spatially independent gauge-coupling [39]. Qualitatively, our results do not depend on this assumption and should apply in any case in which the mass of the W -boson is much less than that of the first gauge-boson KK mode.

\tilde{g} is taken to be much larger than g , so we expand in the small quantity

$$x = \frac{g}{\tilde{g}}. \quad (25)$$

We also find it convenient to define the parameters

$$t = \frac{g'}{g} = \frac{s}{c} \quad (26)$$

where $s^2 + c^2 = 1$. In the continuum limit, $n \rightarrow \infty$, this model reduces to the one described in [39].

The horizontal bars in Figure 4 represent nonlinear sigma models Σ_j which break the gauge symmetry down to electromagnetism

$$G \longrightarrow U(1)_{EM} \quad (27)$$

giving mass to the other $3(n+1)$ gauge bosons. To leading order, the effective Lagrangian for these fields is

$$\mathcal{L}_{D\Sigma} = \frac{f^2}{4} \text{Tr} \left[\sum_j (D_\mu \Sigma_j)^\dagger D^\mu \Sigma_j \right] \quad (28)$$

where

$$D_\mu \Sigma_j = \partial_\mu \Sigma_j + ig_j W_{j,\mu} \Sigma_j - ig_{j+1} \Sigma_j W_{j+1,\mu} \quad (29)$$

with $g_0 = g$, $g_j = \tilde{g}$ and $g_{n+1} = g'$. The nonlinear sigma model fields may be written

$$\Sigma_j = e^{i2\pi_j/f}, \quad (30)$$

in terms of the Goldstone bosons (π_j) which become the longitudinal components of the massive gauge bosons. The π_j and W_j are written in matrix form and are

$$\pi_j = \begin{pmatrix} \frac{1}{2}\pi_j^0 & \frac{1}{\sqrt{2}}\pi_j^+ \\ \frac{1}{\sqrt{2}}\pi_j^- & -\frac{1}{2}\pi_j^0 \end{pmatrix} \quad (31)$$

$$W_{j,\mu} = \begin{pmatrix} \frac{1}{2}W_{j,\mu}^0 & \frac{1}{\sqrt{2}}W_{j,\mu}^+ \\ \frac{1}{\sqrt{2}}W_{j,\mu}^- & -\frac{1}{2}W_{j,\mu}^0 \end{pmatrix} \quad (32)$$

$$W_{n+1,\mu} = \begin{pmatrix} \frac{1}{2}W_{n+1,\mu}^0 & 0 \\ 0 & -\frac{1}{2}W_{n+1,\mu}^0 \end{pmatrix} \quad (33)$$

The mass matrices of the gauge bosons can be obtained by going to unitary gauge ($\Sigma_j \rightarrow 1$). For the neutral gauge bosons, we find

$$M_n^2 = \frac{\tilde{g}^2 f^2}{4} \begin{pmatrix} x^2 & -x & 0 & 0 & \cdot & 0 & 0 \\ -x & 2 & -1 & 0 & \cdot & 0 & 0 \\ 0 & -1 & 2 & -1 & \cdot & 0 & 0 \\ \cdot & \cdot & \cdot & \cdot & \cdot & -1 & 0 \\ 0 & 0 & 0 & \cdot & -1 & 2 & -xt \\ 0 & 0 & 0 & \cdot & 0 & -xt & x^2 t^2 \end{pmatrix} \quad (34)$$

while the matrix M_\pm^2 for the charged gauge bosons is M_n^2 with the last row and column removed.

The photon is massless and given by the wavefunction

$$v_\gamma = \frac{e}{\tilde{g}} \left(\frac{1}{x}, 1, \dots, 1, \frac{1}{xt} \right) \quad (35)$$

where

$$\frac{1}{e^2} = \frac{1}{g^2} + \frac{n}{\tilde{g}^2} + \frac{1}{g'^2}. \quad (36)$$

After diagonalizing the gauge boson mass matrices, we find that the other masses and wavefunctions are given, at leading order in x , by the following expressions. The mass and wavefunction of the light W boson are

$$M_{W0} = \frac{\tilde{g} f x}{2\sqrt{(n+1)}} \quad (37)$$

$$v_{W0}^0 = 1 \quad (38)$$

$$v_{W0}^j = \frac{n-j+1}{n+1} x \quad (39)$$

where the superscript 0 refers to the left-most $SU(2)$ group on the moose while the superscript $j = [1..n]$ refers to the $SU(2)$ gauge groups on the interior of the moose. The masses and wavefunctions of the charged KK modes are

$$M_{Wk} = \frac{\tilde{g} f}{\sqrt{2}} \sqrt{1 - \cos \left[\frac{k\pi}{n+1} \right]} \quad (40)$$

$$v_{Wk}^0 = \frac{-x}{\sqrt{2(n+1)}} \cot \left[\frac{k\pi}{2(n+1)} \right] \quad (41)$$

$$v_{Wk}^j = \sqrt{\frac{2}{n+1}} \sin \left[\frac{jk\pi}{n+1} \right]. \quad (42)$$

Likewise, the mass and wavefunction of the light Z boson are

$$M_{Z0} = \frac{\tilde{g} f x}{2c\sqrt{(n+1)}} \quad (43)$$

$$v_{Z0}^0 = c \quad (44)$$

$$v_{Z0}^j = \frac{c(n+1) - j/c}{n+1} x \quad (45)$$

$$v_{Z0}^{n+1} = -s, \quad (46)$$

where superscript $n+1$ refers to the $U(1)$ group. The

masses and wavefunctions of the neutral KK modes are

$$M_{Zk} = \frac{\tilde{g}f}{\sqrt{2}} \sqrt{1 - \cos \left[\frac{k\pi}{n+1} \right]} = M_{Wk} \quad (47)$$

$$v_{Zk}^0 = \frac{-x}{\sqrt{2(n+1)}} \cot \left[\frac{k\pi}{2(n+1)} \right] \quad (48)$$

$$v_{Zk}^j = \sqrt{\frac{2}{n+1}} \sin \left[\frac{jk\pi}{n+1} \right] \quad (49)$$

$$v_{Zk}^{n+1} = \sqrt{\frac{2}{n+1}} \frac{(-1)^k x}{t} [(n+1)a_1 + b_1] \quad (50)$$

$$a_1 = \frac{(-1)^k}{4(n+1)} \csc^2 \left[\frac{k\pi}{2(n+1)} \right] \quad (51)$$

$$\times \left[(-1)^k \sin \left(\frac{k\pi}{n+1} \right) - t^2 \sin \left(\frac{kn\pi}{n+1} \right) \right]$$

$$b_1 = \frac{-1}{2} \cot \left[\frac{k\pi}{2(n+1)} \right]. \quad (52)$$

We note that the W gauge boson mass is given by

$$M_W = M_{W0} \equiv \frac{gf}{2\sqrt{n+1}} = \frac{gv}{2}, \quad (53)$$

and, hence, we have the relation

$$f = \sqrt{n+1} v. \quad (54)$$

The ratio of the W and Z mass is

$$\frac{M_W}{M_Z} = \frac{M_{W0}}{M_{Z0}} = \frac{1}{c} \quad (55)$$

identifying c with $\cos \theta_W$ at leading order in x .

The ratio of M_W to the mass of the first KK mode M_{W1} is

$$\frac{M_W}{M_{W1}} = \frac{x}{\sqrt{2(n+1)} \left(1 - \cos \left[\frac{\pi}{n+1} \right] \right)} \quad (56)$$

which relates x to the mass ratio M_W/M_{W1} for a given n at leading order. From this we see that expansion in x is justified as long as $M_{W1} \gg M_W$.

B. Fermion Sector

The vertical lines in Figure 4 represent the fermionic fields in the theory. The vertical lines below the circles represent the left chiral fermions while the vertical lines above the circles are the right chiral fermions. Each fermion is in a fundamental representation of the gauge group to which it is attached and a singlet under all the other gauge groups except $U(1)_{n+1}$. The charges under $U(1)_{n+1}$ are as follows: If the fermion is attached to an $SU(2)$ then its charge is $1/3$ for quarks and -1 for leptons. If the fermion is attached to $U(1)_{n+1}$ its charge is twice its electromagnetic charge: 0 for neutrinos, -2

for charged leptons, $4/3$ for up type quarks and $-2/3$ for down type quarks.

The fermions attached to the internal sites ($1 \leq j \leq n$) are vectorially coupled and are, thus, allowed Dirac masses. We take these masses to be common, and denote them by M_F . The symmetries also allow Yukawa couplings of fermions at adjacent sites using the nonlinear sigma fields. We have assumed a very simple form for these couplings, inspired by an extra dimension [70] and represented by the diagonal lines in Figure 4. For simplicity, we take the mass parameter for all the diagonal Yukawa links – *except* for the two at the ends of the diagram – to be M_F , the same as the Dirac mass, corresponding to a massless fermion in a five-dimensional model. The Yukawa links on the ends are taken to be suppressed by factors of ϵ_L on the left end and ϵ_R on the right end. All together, the masses of the fermions and the leading order interactions of the fermions and nonlinear sigma fields are given by

$$\begin{aligned} \mathcal{L}_{\psi\Sigma} = & -M_F \left[\epsilon_L \bar{\psi}_{L0} \Sigma_0 \psi_{R1} - \sum_j \bar{\psi}_{Lj} \psi_{Rj} \right. \\ & \left. + \sum_j \bar{\psi}_{Lj} \Sigma_j \psi_{R,j+1} + \bar{\psi}_{Ln} \epsilon_R \Sigma_n \psi_{R,n+1} + h.c. \right] \end{aligned} \quad (57)$$

where the value of ϵ_L is the same for all fermions, while ϵ_R is a diagonal matrix which distinguishes flavors [33, 49]. For example for the top and bottom quark we have

$$\epsilon_R = \begin{pmatrix} \epsilon_{Rt} & 0 \\ 0 & \epsilon_{Rb} \end{pmatrix} \quad (58)$$

The fermion mass matrix can be diagonalized by performing unitary transformations on the left- and right-handed fermions separately. To leading order in $\epsilon_{L,R}$ we find the following masses and wavefunctions for the lightest fermion, F_0 , in a given tower (which we associate with an ordinary standard model fermion)

$$M_{F_0} = M_F \epsilon_L \epsilon_{Rf} \quad (59)$$

$$v_{LF_0}^0 = 1 \quad (60)$$

$$v_{LF_0}^j = \epsilon_L \quad (61)$$

$$v_{RF_0}^j = \epsilon_{Rf} \quad (62)$$

$$v_{RF_0}^{n+1} = 1 \quad (63)$$

while the expressions for the heavier states, F_k , are

$$M_{F_k} = 2M_F \cos \left[\frac{(n-k+1)\pi}{2n+1} \right] \quad (64)$$

$$v_{LF_k}^0 = \frac{\epsilon_L}{\sqrt{2n+1}} \tan \left[\frac{(n-k+1)\pi}{2n+1} \right] \quad (65)$$

$$v_{LF_k}^j = \frac{2(-1)^j}{\sqrt{2n+1}} \sin \left[\frac{2j(n-k+1)\pi}{2n+1} \right] \quad (66)$$

$$v_{RF_k}^j = \frac{(-1)^{n+k+j+1} 2}{\sqrt{2n+1}} \sin \left[\frac{2(n-j+1)(n-k+1)\pi}{2n+1} \right] \quad (67)$$

$$v_{RF_k}^{n+1} = \frac{(-1)^k \epsilon_{R_f}}{\sqrt{2n+1}} \tan \left[\frac{(n-k+1)\pi}{2n+1} \right] \quad (68)$$

For small ϵ_L , we see that the left-handed component of the lightest fermion in each tower is primarily located at site 0 – and the flavor-universal factor ϵ_L controls the amount of fermion “delocalization” along the moose. Likewise, the right-handed component is primarily located at site $n+1$, and the flavor-dependent quantities ϵ_{R_f} control the degree of delocalization. Since the amplitude for $t\bar{t} \rightarrow W^+W^-$ scattering will depend on the values of ϵ_L and ϵ_{R_t} , we need to evaluate these quantities; we will start with ϵ_L and then use it to constrain ϵ_{R_t} .

Precision electroweak corrections provide a useful source of constraints on the parameters of Higgsless models. While custodial symmetry generally keeps the tree-level value of $\Delta\rho = \alpha T$ sufficiently small, satisfying the bounds on S at tree level requires some degree of fermion delocalization [35, 36, 37, 38, 39, 40, 41, 42]. In a general Higgsless model, one can calculate the “ideal delocalization” profile of a fermion along the moose that guarantees S and other precision corrections will vanish at tree level. However, the $n(+2)$ -site model studied here and in [49] has been simplified such that the light fermion profile is strictly flat on the interior of the moose (*c.f.* Eqns. (60) - (63)), rather than being “ideal”. We therefore quantify the relationship between delocalization (ϵ_L) and S in this model by studying a particular experimental observable.

The coupling $g_{W_{ev}}$ between the W , electron and electron-neutrino is well-measured and lies close to the SM value. One may parameterize the deviation in this coupling from the SM value as

$$g_{W_{ev}} = g_{W_{evSM}} (1 + aS + bT + cU) \quad (69)$$

where a , b and c are $O(\alpha)$ parameters. We have already noted that custodial symmetry makes T small in this model and U is generally suppressed relative to both S and T . Hence, the largest corrections are due to S :

$$g_{W_{ev}} \simeq g_{W_{evSM}} (1 + aS). \quad (70)$$

We can ensure $S \simeq 0$ at tree level by requiring $g_{W_{ev}}$ in the $n(+2)$ -site model to be the same as in the standard model. An explicit calculation of $g_{W_{ev}}$ in this model,

which requires expanding the wavefunctions, masses, and couplings to order ϵ_L^2 and order x^2 , yields [49]

$$g_{W_{evn}} = g_{W_{evSM}} \left(1 + \frac{n(n+2)}{6(n+1)} x^2 - \frac{n}{2} \epsilon_L^2 \right). \quad (71)$$

Therefore, the condition

$$\epsilon_L^2 = \frac{n+2}{3(n+1)} x^2 \quad (72)$$

causes S to vanish at tree-level. Using Eqn. (56) this is equivalent to

$$\epsilon_L^2 = \frac{2}{3} (n+2) \left(1 - \cos \left[\frac{\pi}{n+1} \right] \right) \frac{M_W^2}{M_{W_1}^2}, \quad (73)$$

in terms of physical masses. Here again, note that ϵ_L is small so long as $M_W \ll M_{W_1}$.

Finally, the parameter ϵ_{R_f} can be determined by taking the ratio of the masses of the light fermion and the first KK mode.

$$\frac{M_{F_0}}{M_{F_1}} = \frac{\epsilon_L \epsilon_{R_f}}{2 \cos \left[\frac{n\pi}{2n+1} \right]} \quad (74)$$

Since we know ϵ_L , this gives a prediction for ϵ_{R_f} in terms of physical masses

$$\epsilon_{R_f} = \frac{\sqrt{6} \cos \left[\frac{n\pi}{2n+1} \right]}{\sqrt{(n+2) \left(1 - \cos \left[\frac{\pi}{n+1} \right] \right)}} \frac{M_{F_0}}{M_{F_1}} \frac{M_{W_1}}{M_W}. \quad (75)$$

For all flavors except the top quark, this parameter is tiny; at leading order, we therefore set $\epsilon_{R_f} = 0$ for all the light fermions. The size of ϵ_{R_t} affects $\Delta\rho$ at one loop; comparison of the experimental bounds on $\Delta\rho$ with the value calculated in Higgsless models [33, 49] shows that ϵ_{R_t} must also be relatively small. In what follows, we therefore keep only the leading terms in ϵ_{R_t} .

C. Goldstone Boson Sector

We will perform the computation of the process $t_+ \bar{t}_+ \rightarrow W_L^+ W_L^-$ in the $n(+2)$ site model using the equivalence theorem. We must, therefore, determine the wavefunction of the Goldstone bosons associated with (eaten by) the massive gauge bosons. This is determined by the mixing between the two given in Eqn. (28). To find the mixing, we expand the nonlinear sigma-model field Σ_j and keep the terms linear in both the gauge bosons (W_j) and the Goldstone bosons (π_j). After these manipulations, Eqn. (28) becomes

$$\mathcal{L}_{\pi W} = -i \frac{\tilde{g}f}{2} \left[\begin{aligned} & \left\{ \partial_\mu \pi_0, x W_0^\mu - W_1^\mu \right\} \\ & + \sum_{j=1}^{n-1} \left\{ \partial_\mu \pi_j, W_j^\mu - W_{j+1}^\mu \right\} \\ & + \left\{ \partial_\mu \pi_n, W_n^\mu - xt W_{n+1}^\mu \right\} \end{aligned} \right] \quad (76)$$

from which we may read off the wavefunctions for the charged Goldstone bosons as

$$v_{\pi_k^\pm}^{[0]} = \frac{1}{N_{\pi_k^\pm}} (x v_{W_k}^0 - v_{W_k}^1) \quad (77)$$

$$v_{\pi_k^\pm}^{[j]} = \frac{1}{N_{\pi_k^\pm}} (v_{W_k}^j - v_{W_k}^{j+1}) \quad (78)$$

$$v_{\pi_k^\pm}^{[n]} = \frac{1}{N_{\pi_k^\pm}} v_{W_k}^n \quad (79)$$

where the N_{π_k} are normalization factors. Note that Nambu-Goldstone boson components are associated with the links rather than the gauge groups: the superscript [0] refers to the left-most link, the superscript [n] refers to the right-most link, and the superscripts [j] range from 1 through n-1 and denote the interior links of the Moose. The wavefunctions for the neutral Goldstone bosons are similar

$$v_{\pi_k^0}^{[0]} = \frac{1}{N_{\pi_k^0}} (x v_{Z_k}^0 - v_{Z_k}^1) \quad (80)$$

$$v_{\pi_k^0}^{[j]} = \frac{1}{N_{\pi_k^0}} (v_{Z_k}^j - v_{Z_k}^{j+1}) \quad (81)$$

$$v_{\pi_k^0}^{[n]} = \frac{1}{N_{\pi_k^0}} (v_{Z_k}^n - x t v_{Z_k}^{n+1}), \quad (82)$$

but include a contribution from the Z_k wavefunction on the $U(1)$ site.

These wavefunctions are particularly simple for the lightest modes, the W and Z : they are flat

$$v_{\pi_0^\pm}^{[l]} = \frac{1}{\sqrt{n+1}} = v_{\pi_0^0}^{[l]} \quad (83)$$

with the same value on all links [$l = 0 \dots n$] of the Moose.

D. Couplings

To obtain the couplings of the Goldstone bosons to the fermions, we start from Eqn. (58), expand the nonlinear sigma-model fields, and plug in the eigenmode wavefunctions we have just derived. Doing this, we find

$$\begin{aligned} g_{LtF_k\pi} &= -i \frac{\sqrt{2} M_F}{f} \left[\epsilon_L v_{Lt}^0 v_{RF_k}^1 v_\pi^{[0]} + \sum_i v_{Lt}^i v_{RF_k}^{i+1} v_\pi^{[i]} \right. \\ &\quad \left. + \epsilon_R b v_{Lt}^n v_{RF_k}^{n+1} v_\pi^{[n]} \right] \\ &= (-1)^k \frac{i\sqrt{2} M_F \epsilon_L}{\sqrt{2n+1}(n+1)v} \tan \left[\frac{(n-k+1)\pi}{2n+1} \right] \quad (84) \end{aligned}$$

$$\begin{aligned} g_{RtF_k\pi} &= -i \frac{\sqrt{2} M_F}{f} \left[\epsilon_L v_{LF_k}^0 v_{Rt}^1 v_\pi^{[0]} + \sum_i v_{LF_k}^i v_{Rt}^{i+1} v_\pi^{[i]} \right. \\ &\quad \left. + \epsilon_R t v_{LF_k}^n v_{Rt}^{n+1} v_\pi^{[n]} \right] \\ &= \frac{i\sqrt{2} M_F \epsilon_R}{\sqrt{2n+1}(n+1)v} \tan \left[\frac{(n-k+1)\pi}{2n+1} \right] \quad (85) \end{aligned}$$

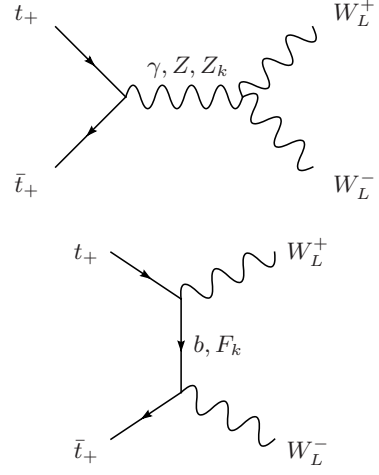


FIG. 5: The diagrams that contribute to the process $t_+ \bar{t}_+ \rightarrow W_L^+ W_L^-$ in the $n(+2)$ site Higgsless model. There are analogous diagrams for the process $t_- \bar{t}_- \rightarrow W_L^+ W_L^-$. As in the SM, most of the linear growth in \sqrt{s} will cancel. All the persisting linear growth in \sqrt{s} comes from the t channel diagrams.

$$\begin{aligned} g_{tt\pi^+\pi^-} &= \frac{M_F}{f^2} \left[\epsilon_L v_{Lt}^0 v_{Rt}^1 (v_\pi^{[0]})^2 + \sum_i v_{Lt}^i v_{Rt}^{i+1} (v_\pi^{[i]})^2 \right. \\ &\quad \left. + \epsilon_R t v_{Lt}^n v_{Rt}^{n+1} (v_\pi^{[n]})^2 \right] \\ &= \frac{m_t}{(n+1)v^2}. \quad (86) \end{aligned}$$

Here we have denoted the lightest fermions (previously denoted F_0) by t and b , as appropriate, while leaving the corresponding KK modes as F_k (which, to leading order in $\epsilon_{L,R}$, have the same properties for all quarks). Note that the four point vertex has an extremely simple form, and vanishes in the limit $n \rightarrow \infty$.

IV. UNITARITY BOUNDS ON $t\bar{t} \rightarrow W_L W_L$

The diagrams that contribute at tree level to $t_+ \bar{t}_+ \rightarrow W_L^+ W_L^-$ are shown in Figure 5. We are again interested in the behavior at large energies, so we expand in the small parameters M_W^2/s and m_t^2/s ; we also include all colors and both helicity polarizations in a coupled channel analysis (Eqn. (8)). The calculation is most easily performed using the equivalence theorem [11, 68]. Again, as in the SM (see Figure 3), the potential s -channel diagrams do not contribute to the $J = 0$ amplitude, and the only diagrams that contribute are shown in Figure 6. The scattering amplitude arising from the diagrams in Figure 6 is

$$\mathcal{M} = \sqrt{6s} \left(g_{tt\pi^+\pi^-} - \sum_k \frac{M_{F_k} g_{LtF_k\pi} g_{RtF_k\pi}}{t - M_{F_k}^2} \right) \quad (87)$$

where the couplings are given in Eqns. (84) – (86).

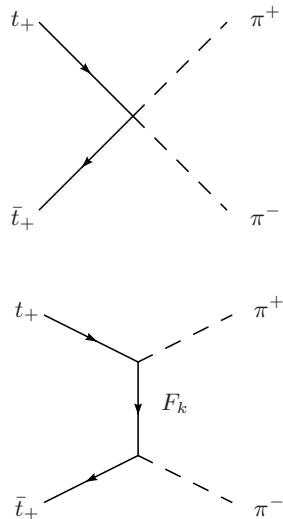


FIG. 6: Diagrams contributing to unitarity violation at high energies in the process $t_+ \bar{t}_+ \rightarrow \pi^+ \pi^-$. There are analogous diagrams for the process $t_- \bar{t}_- \rightarrow \pi^+ \pi^-$. The top diagram grows linearly with \sqrt{s} for all energies, whereas the bottom diagrams only grow with \sqrt{s} up to M_{F_k} , after which they fall off as $1/\sqrt{s}$.

The $J = 0$ partial wave can be extracted as

$$a_0 = \frac{1}{32\pi} \int_{-1}^1 d \cos \theta \mathcal{M} \quad (88)$$

$$= \frac{\sqrt{6}}{16\pi} \left[g_{tt\pi^+\pi^-} \sqrt{s} + \sum_k g_{LtF_k\pi} g_{RtF_k\pi} g \left(\frac{\sqrt{s}}{M_{F_k}} \right) \right]$$

where

$$g(x) = \frac{1}{x} \ln(1 + x^2) \quad (89)$$

This partial wave must be less than $1/2$ to maintain unitarity, giving a bound on \sqrt{s} and/or M_{F_1} . We have plotted this bound in Figures 7 and 8 for $n = 0, 1, 2, \dots, 10, 20, 30$ and ∞ . The $n = 0$ bound corresponds to the original AC bound of Eqn. (23).

We see from these figures that there are two important domains corresponding to different ranges of values for M_{F_1} . In the first domain, where $M_{F_1} \lesssim 4.5$ TeV, we find that unitarity can be satisfied up to very large energies. In this limit, we find that the t channel diagram becomes irrelevant and the process is controlled by the four point vertex (Figure 6). For the lowest fermion masses, $M_{F_1} \ll 4.5$ TeV, we find

$$a_0 \simeq \frac{\sqrt{6} s m_t}{16\pi v^2 (n+1)} \lesssim \frac{1}{2} \quad (90)$$

which gives the bound

$$\sqrt{s} \lesssim (n+1) 3.5 \text{ TeV} \quad (91)$$

In this “low” KK fermion-mass region, unitarity is valid to approximately $(n+1)$ times the AC bound.

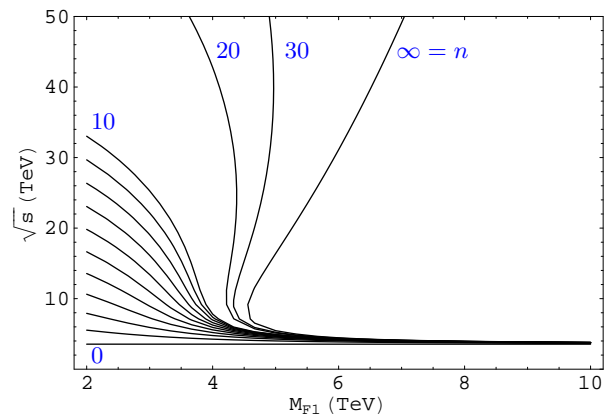


FIG. 7: The scale where unitarity breaks down in the helicity nonconserving channel in the $n(+2)$ site model. Unitarity is valid in the region below and to the left of a given curve. The bottom-most curve is for $n = 0$ and is the AC bound. The line directly above the bottom one is for $n = 1$ and corresponds to the Three Site Model. The line directly above that is for $n = 2$ and so on until $n = 10$. The line above that is for $n = 20$, the line to the right of that is for $n = 30$ and the line to the right of that is the continuum limit ($n \rightarrow \infty$). We find that unitarity breaks down if either E is large or M_{F_1} is large. If M_{F_1} is large, then unitarity breaks down for \sqrt{s} very close to the AC bound. On the other hand, if $M_{F_1} \lesssim 4.5$ TeV, unitarity can be valid in this process to very high energies, with the precise value depending on the number of sites n .

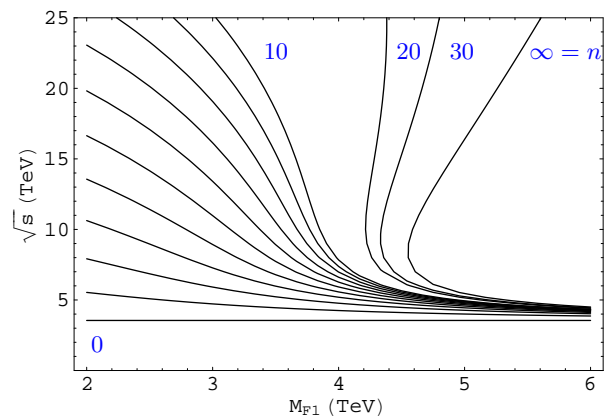


FIG. 8: Expanded view of low \sqrt{s} region of Figure 7.

In the second domain, where $M_{F_1} > 4.5$ TeV, we find that, for all n , unitarity breaks down at a value of \sqrt{s} given approximately by the AC bound (Eqn. (23)). In Figures 7 and 8, we see that at $M_{F_1} \sim 4.5$ TeV, the curves corresponding to small n approach the $n = 0$ curve, while the curves for large n turn back on themselves, defining a wedge-shaped area in which unitarity is always violated starting at \sqrt{s} of order a few TeV.

To understand why $M_{F_1} = 4.5$ TeV is the fermion mass value at which the theory crosses from the first to the second domain, we consider what happens as $n \rightarrow \infty$. In

this limit, the four point vertex disappears and we are left with the partial wave amplitude

$$\lim_{n \rightarrow \infty} a_0 = \frac{2\sqrt{6}M_{F_1}m_t}{\pi^4 v^2} \sum_k \frac{(-1)^{k+1}}{(2k-1)^2} g\left(\frac{\sqrt{s}}{(2k-1)M_{F_1}}\right). \quad (92)$$

This sum is dominated by the first KK mode ($k=1$). Thus, to locate the left most edge of the wedge-shaped in the (\sqrt{s}, M_{F_1}) plane where unitarity is violated, we need only keep the first KK fermion mode

$$\lim_{n \rightarrow \infty} a_0(k=1) \approx \frac{2\sqrt{6}M_{F_1}m_t}{\pi^4 v^2} g\left(\frac{\sqrt{s}}{M_{F_1}}\right). \quad (93)$$

The function $g(\sqrt{s}/M_{F_1})$ determines the shape of this bound. It is maximized for $\sqrt{s} = 2M_{F_1}$ and gives the upper limit of M_{F_1} ,

$$M_{F_1} \lesssim \frac{\pi^4 v^2}{2\sqrt{6}m_t \ln(5)} \sim 4.25 \text{ TeV}, \quad (94)$$

if we want this amplitude to be unitary up to very high scales. Including the higher fermion KK modes changes this upper bound only slightly, to ~ 4.5 TeV. Note that, in the continuum limit, the scattering amplitude does not grow at asymptotically high energies – a property ensured by various sum-rules satisfied by the couplings [71, 72]. Nonetheless, as illustrated in Figures 7 and 8, the properly normalized spin-0 coupled-channel amplitude exceeds the unitarity bound for various ranges of \sqrt{s} and M_{F_1} .

While our work demonstrates that the bound on the scale of fermion mass generation is independent of the bound on the scale of gauge-boson mass generation in these models, the physical significance of the fermion-mass-generation bound depends on the “high-energy” (UV) completion which underlies the $n(+2)$ site model. The simplest possible UV completion is one in which each of the nonlinear sigma-model link theories is replaced by a linear Gell-mann–Levy sigma model. In this case, the

strength of the adjacent site couplings in Eqn. (57) is determined by a dimensionless Yukawa coupling of order M_F/f . The large- M_F limit, therefore, corresponds to large Yukawa coupling. In this case, the bound on M_F is expected to be related to the triviality bound on the corresponding Yukawa coupling [66, 67, 73].

V. SUMMARY

In this paper we have examined upper bounds on the scale of top-quark mass generation in viable deconstructed Higgsless models. These bounds are derived from the scale at which unitarity is violated in the helicity nonconserving amplitude for top-anti-top pairs to scatter into pairs of longitudinally polarized electroweak gauge bosons. We have shown that the scale of unitarity violation in this process depends on the mass of the additional vector-like fermion states that occur in these theories and, in this sense, the scale of fermion mass generation is *separate* from that of gauge-boson mass generation. For sufficiently light vector fermions, and for a deconstructed theory with sufficiently many lattice sites (that is, sufficiently close to the continuum limit), we have shown that the Appelquist-Chanowitz bound on top-quark mass generation is substantially weakened, while the bound is recovered as one increases the mass of the vector-like fermions. Our results are expected to apply to any model in which top-quark mass generation occurs, in part, through mixing between chiral and vector fermions.

VI. ACKNOWLEDGEMENTS

This work was supported in part by the US National Science Foundation under grant PHY-0354226. We thank Stefano DiChiara and Hong-Jian He for useful conversations.

-
- [1] P. W. Higgs, Phys. Lett. **12**, 132 (1964).
 - [2] S. Weinberg, Phys. Rev. Lett. **19**, 1264 (1967).
 - [3] A. Salam, 1968.
 - [4] T. Appelquist and M. S. Chanowitz, *Unitarity Bound on the Scale of Fermion Mass Generation*, Phys. Rev. Lett. **59**, 2405 (1987) [Erratum-ibid. **60**, 1589 (1988)].
 - [5] W. J. Marciano, G. Valencia and S. Willenbrock, Phys. Rev. D **40**, 1725 (1989).
 - [6] M. Golden, Phys. Lett. B **338**, 295 (1994) [arXiv:hep-ph/9408272].
 - [7] F. Maltoni, J. M. Niczyporuk and S. Willenbrock, Phys. Rev. D **65**, 033004 (2002) [arXiv:hep-ph/0106281].
 - [8] D. A. Dicus and H. J. He, Phys. Rev. D **71**, 093009 (2005) [arXiv:hep-ph/0409131].
 - [9] C. H. Llewellyn Smith, Phys. Lett. B **46**, 233 (1973).
 - [10] D. A. Dicus and V. S. Mathur, Phys. Rev. D **7**, 3111 (1973).
 - [11] J. M. Cornwall, D. N. Levin and G. Tiktopoulos, Phys. Rev. D **10**, 1145 (1974) [Erratum-ibid. D **11**, 972 (1975)].
 - [12] B. W. Lee, C. Quigg and H. B. Thacker, Phys. Rev. D **16**, 1519 (1977).
 - [13] M. J. G. Veltman, Acta Phys. Polon. B **8**, 475 (1977).
 - [14] C. Csaki, C. Grojean, H. Murayama, L. Pilo and J. Terning, *Gauge theories on an interval: Unitarity without a Higgs*, Phys. Rev. D **69**, 055006 (2004) [arXiv:hep-ph/0305237].
 - [15] R. Sekhar Chivukula, D. A. Dicus, and H.-J. He, *Unitarity of compactified five dimensional yang-mills theory*, Phys. Lett. **B525** (2002) 175–182, [arXiv:hep-ph/0111016].

- [16] R. S. Chivukula and H.-J. He, *Unitarity of deconstructed five-dimensional yang-mills theory*, *Phys. Lett.* **B532** (2002) 121–128, [arXiv:hep-ph/0201164].
- [17] R. S. Chivukula, D. A. Dicus, H.-J. He, and S. Nandi, *Unitarity of the higher dimensional standard model*, *Phys. Lett.* **B562** (2003) 109–117, [arXiv:hep-ph/0302263].
- [18] H.-J. He, *Higgsless deconstruction without boundary condition*, arXiv:hep-ph/0412113.
- [19] I. Antoniadis, *Phys. Lett. B* **246**, 377 (1990).
- [20] K. Agashe, A. Delgado, M. J. May and R. Sundrum, *RS1, Custodial Isospin and Precision Tests*, *JHEP* **0308**, 050 (2003) [arXiv:hep-ph/0308036].
- [21] C. Csaki, C. Grojean, L. Pilo, and J. Terning, *Towards a realistic model of higgsless electroweak symmetry breaking*, *Phys. Rev. Lett.* **92** (2004) 101802, [arXiv:hep-ph/0308038].
- [22] G. Burdman and Y. Nomura, *Holographic theories of electroweak symmetry breaking without a Higgs boson*, *Phys. Rev. D* **69**, 115013 (2004) [arXiv:hep-ph/0312247].
- [23] G. Cacciapaglia, C. Csaki, C. Grojean and J. Terning, *Oblique corrections from Higgsless models in warped space*, *Phys. Rev. D* **70**, (2004) 075014, [arXiv:hep-ph/0401160].
- [24] N. Arkani-Hamed, A. G. Cohen, and H. Georgi, *(de)constructing dimensions*, *Phys. Rev. Lett.* **86** (2001) 4757–4761, [arXiv:hep-th/0104005].
- [25] C. T. Hill, S. Pokorski, and J. Wang, *Gauge invariant effective lagrangian for kaluza-klein modes*, *Phys. Rev.* **D64** (2001) 105005, [arXiv:hep-th/0104035].
- [26] R. Foadi, S. Gopalakrishna, and C. Schmidt, *Higgsless electroweak symmetry breaking from theory space*, *JHEP* **03** (2004) 042, [arXiv:hep-ph/0312324].
- [27] J. Hirn and J. Stern, *The role of spurions in Higgs-less electroweak effective theories*, *Eur. Phys. J. C* **34**, 447 (2004) [arXiv:hep-ph/0401032].
- [28] R. Casalbuoni, S. De Curtis and D. Dominici, *Moose models with vanishing S parameter*, *Phys. Rev. D* **70** (2004) 055010 [arXiv:hep-ph/0405188].
- [29] R. S. Chivukula, E. H. Simmons, H. J. He, M. Kurachi and M. Tanabashi, *The structure of corrections to electroweak interactions in Higgsless models*, *Phys. Rev. D* **70** (2004) 075008 [arXiv:hep-ph/0406077].
- [30] M. Perelstein, *Gauge-assisted technicolor?*, *JHEP* **10** (2004) 010, [arXiv:hep-ph/0408072].
- [31] H. Georgi, *Fun with Higgsless theories*, *Phys. Rev. D* **71**, 015016 (2005) [arXiv:hep-ph/0408067].
- [32] R. Sekhar Chivukula, E. H. Simmons, H. J. He, M. Kurachi and M. Tanabashi, *Electroweak corrections and unitarity in linear moose models*, *Phys. Rev. D* **71** (2005) 035007 [arXiv:hep-ph/0410154].
- [33] R. Sekhar Chivukula, B. Coleppa, S. Di Chiara, E. H. Simmons, H. J. He, M. Kurachi and M. Tanabashi, “A three site higgsless model,” arXiv:hep-ph/0607124.
- [34] R. Casalbuoni, S. De Curtis, D. Dominici and R. Gatto, *Phys. Lett. B* **155**, 95 (1985).
- [35] L. Anichini, R. Casalbuoni and S. De Curtis, *Phys. Lett. B* **348**, 521 (1995) [arXiv:hep-ph/9410377].
- [36] G. Cacciapaglia, C. Csaki, C. Grojean and J. Terning, *Curing the ills of Higgsless models: The S parameter and unitarity*, *Phys. Rev. D* **71** (2005) 035015 [arXiv:hep-ph/0409126].
- [37] G. Cacciapaglia, C. Csaki, C. Grojean, M. Reece and J. Terning, *Top and bottom: A brane of their own*, *Phys. Rev. D* **72**, (2005) 095018 [arXiv:hep-ph/0505001].
- [38] R. Foadi, S. Gopalakrishna and C. Schmidt, *Effects of fermion localization in Higgsless theories and electroweak constraints*, *Phys. Lett. B* **606** (2005) 157 [arXiv:hep-ph/0409266].
- [39] R. Foadi and C. Schmidt, *An Effective Higgsless Theory: Satisfying Electroweak Constraints and a Heavy Top Quark*, *Phys. Rev. D* **73** (2006) 075011 [arXiv:hep-ph/0509071].
- [40] R. S. Chivukula, E. H. Simmons, H. J. He, M. Kurachi and M. Tanabashi, *Deconstructed Higgsless models with one-site delocalization*, *Phys. Rev. D* **71**, 115001 (2005) [arXiv:hep-ph/0502162].
- [41] R. Casalbuoni, S. De Curtis, D. Dolce and D. Dominici, *Playing with fermion couplings in Higgsless models*, *Phys. Rev. D* **71**, 075015 (2005) [arXiv:hep-ph/0502209].
- [42] R. Sekhar Chivukula, E. H. Simmons, H. J. He, M. Kurachi and M. Tanabashi, *Ideal fermion delocalization in Higgsless models*, *Phys. Rev. D* **72**, 015008 (2005) [arXiv:hep-ph/0504114].
- [43] M. E. Peskin and T. Takeuchi, *Estimation of oblique electroweak corrections*, *Phys. Rev.* **D46** (1992) 381–409.
- [44] G. Altarelli and R. Barbieri, *Vacuum polarization effects of new physics on electroweak processes*, *Phys. Lett.* **B253** (1991) 161–167.
- [45] G. Altarelli, R. Barbieri, and S. Jadach, *Toward a model independent analysis of electroweak data*, *Nucl. Phys.* **B369** (1992) 3–32.
- [46] R. Barbieri, A. Pomarol, R. Rattazzi and A. Strumia, *Electroweak symmetry breaking after LEP1 and LEP2*, *Nucl. Phys. B* **703**, 127 (2004) [arXiv:hep-ph/0405040].
- [47] R. S. Chivukula, E. H. Simmons, H.-J. He, M. Kurachi, and M. Tanabashi, *Universal non-oblique corrections in higgsless models and beyond*, *Phys. Lett.* **B603** (2004) 210–218, [arXiv:hep-ph/0408262].
- [48] R. Sekhar Chivukula, E. H. Simmons, H. J. He, M. Kurachi and M. Tanabashi, *Phys. Rev. D* **75**, 035005 (2007) [arXiv:hep-ph/0612070].
- [49] B. Coleppa, S. Di Chiara and R. Foadi, *One loop corrections to the rho parameter in Higgsless models*, arXiv:hep-ph/0612213.
- [50] B. A. Dobrescu and C. T. Hill, *Electroweak symmetry breaking via top condensation seesaw*, *Phys. Rev. Lett.* **81**, 2634 (1998) [arXiv:hep-ph/9712319].
- [51] R. S. Chivukula, B. A. Dobrescu, H. Georgi and C. T. Hill, *Top quark seesaw theory of electroweak symmetry breaking*, *Phys. Rev. D* **59**, 075003 (1999) [arXiv:hep-ph/9809470].
- [52] H. J. He, C. T. Hill and T. M. P. Tait, *Top quark seesaw, vacuum structure and electroweak precision constraints*, *Phys. Rev. D* **65**, 055006 (2002) [arXiv:hep-ph/0108041].
- [53] M. Suzuki, *Phys. Rev. D* **44**, 3628 (1991).
- [54] R. F. Lebed and M. Suzuki, *Phys. Rev. D* **45**, 1744 (1992).
- [55] D. B. Kaplan, *Nucl. Phys. B* **365**, 259 (1991).
- [56] J. M. Maldacena, *The large n limit of superconformal field theories and supergravity*, *Adv. Theor. Math. Phys.* **2** (1998) 231–252, [hep-th/9711200].
- [57] S. S. Gubser, I. R. Klebanov, and A. M. Polyakov, *Gauge theory correlators from non-critical string theory*, *Phys. Lett.* **B428** (1998) 105–114, [hep-th/9802109].
- [58] E. Witten, *Anti-de sitter space and holography*, *Adv. Theor. Math. Phys.* **2** (1998) 253–291, [hep-th/9802150].
- [59] O. Aharony, S. S. Gubser, J. M. Maldacena, H. Ooguri,

- and Y. Oz, *Large n field theories, string theory and gravity*, *Phys. Rept.* **323** (2000) 183–386, [[hep-th/9905111](#)].
- [60] C. Csaki, J. Hubisz and P. Meade, [arXiv:hep-ph/0510275](#).
- [61] T. Appelquist and C. W. Bernard, *The Nonlinear Sigma Model In The Loop Expansion*, *Phys. Rev. D* **23**, 425 (1981).
- [62] T. Appelquist and C. W. Bernard, *Strongly Interacting Higgs Bosons*, *Phys. Rev. D* **22**, 200 (1980).
- [63] A. C. Longhitano, *Phys. Rev. D* **22**, 1166 (1980).
- [64] A. C. Longhitano, *Low-Energy Impact Of A Heavy Higgs Boson Sector*, *Nucl. Phys. B* **188**, 118 (1981).
- [65] T. Appelquist and G. H. Wu, *The Electroweak chiral Lagrangian and new precision measurements*, *Phys. Rev. D* **48**, 3235 (1993) [[arXiv:hep-ph/9304240](#)].
- [66] M. S. Chanowitz, M. A. Furman and I. Hinchliffe, *Phys. Lett. B* **78**, 285 (1978).
- [67] M. S. Chanowitz, M. A. Furman and I. Hinchliffe, *Nucl. Phys. B* **153**, 402 (1979).
- [68] C. E. Vayonakis, *Lett. Nuovo Cim.* **17**, 383 (1976).
- [69] H. Georgi, *Nucl. Phys. B* **266**, 274 (1986).
- [70] C. T. Hill and A. K. Leibovich, *Phys. Rev. D* **66**, 016006 (2002) [[arXiv:hep-ph/0205057](#)].
- [71] C. Schwinn, *Phys. Rev. D* **69**, 116005 (2004) [[arXiv:hep-ph/0402118](#)].
- [72] C. Schwinn, *Phys. Rev. D* **71**, 113005 (2005) [[arXiv:hep-ph/0504240](#)].
- [73] M. B. Einhorn and G. J. Goldberg, *Phys. Rev. Lett.* **57**, 2115 (1986).